Compatibility of Steels at 450°-650°C in Supercritical CO_2 with O_2 and H_2O Additions

B. A. Pint, M. J. Lance, R. Pillai and J. R. Keiser
Corrosion Science and Technology Group, Materials Science and Technology Division
Oak Ridge National Laboratory, Oak Ridge, TN 37831-6156 USA

ABSTRACT

Direct-fired supercritical CO_2 (sCO_2) power cycles are being commercialized to revolutionize the use of fossil fuels as a low-emission power source. However, the cycle will increase O_2 and H_2O in the sCO_2 and the implications of these additions have not been fully studied, particularly for lower cost steels that are needed in the lower temperature segments of the plant. Representative 9 and 12%Cr ferritic-martensitic (FM) steels and conventional and advanced austenitic steels were evaluated at 450-650°C in sCO_2 with 1%O_2 and 0.1%H_2O at 300 bar to determine their maximum use temperatures. Compared to research grade (low impurity) sCO_2 in indirect-fired cycles, the mass gains and scale thickness were not significantly changed for FM steels: both formed thick duplex Fe-rich scales with and without impurities. For austenitic steels, higher mass gains were observed at all temperatures with increased Fe-rich oxide nodule formation. After 1000 h at 650°C, the measured bulk C content was high for all of the steels with the addition of impurities suggesting a lower maximum operating temperature for steels. The impact of the environment on the post-exposure room temperature tensile properties was also evaluated and compared to 1000 h Ar anneals.

Keywords: supercritical carbon dioxide, steels, impurities, carbon ingress

INTRODUCTION

Using supercritical CO_2 (sCO_2) as a working fluid is being explored for a number of power generation technologies including fossil, nuclear, geothermal, concentrating solar power (CSP) and waste heat recovery[1-7]. The various sCO_2 cycles are attractive because of the low critical point (31°C/73.8 bar) and the reduced work of compression compared to an ideal gas. While CO_2 is sometimes described as inert, there is a long history of component degradation in subcritical and supercritical CO_2 and a particular concern about internal carburization[8-16]. Recent work has found that Ni-based alloys appear to have good compatibility with sCO_2 up to 800°C[14,17-21]. However, less expensive steels would be desirable for components operating at ≤650°C. Prior experience with low-alloy and ferritic-martensitic (FM) steels (e.g. Grade 9, K90941) in the UK advanced gas cooled reactors (AGRs) showed breakaway

oxidation associated with internal carburization for operation in 43 bar CO_2 at <550°C[15,22]. A recent review concluded that 9-12%Cr creep-strength enhanced FM steels were limited to 450°C in sCO_2[16], substantially lower than the 580°-600°C limit in supercritical steam[23]. However, CO_2 additions (CH_4, H_2O, etc.) used in AGRs to prevent oxidation of the graphite moderator may have negatively affected performance by increasing the C activity compared to low impurity CO_2.

For combusting fossil fuels, the direct-fired oxy-combustion or Allam cycle[3,5,7] represents a potentially attractive strategy for carbon capture, utilization and storage. However, the high O_2 and H_2O impurity levels compared to indirect-fired closed sCO_2 cycles is a further concern. Initial studies of the effect of sCO_2 impurities at >650°C indicated that impurities accelerate reaction rates[18,20]. To further explore the effects of impurities and establish maximum operating temperatures in sCO_2, the current ongoing study exposed two FM steels and two austenitic steels to 300 bar RG sCO_2 at 450°-650°C for 1000 h (two 500-h cycles) with and without controlled O_2 and H_2O additions[20] to simulate expected conditions in the Allam cycle. Mass change, oxide thickness, room temperature tensile properties, bulk C content[8,9] and C profiles were measured to assess reaction kinetics and internal carburization with and without impurities.

EXPERIMENTAL PROCEDURE

Table 1 lists the measured chemical composition of the four steels used in this study. Steel coupons (~12 x 20 x 1.5mm) were machined and polished to a 600 grit finish and SS-3 type[24] dogbone tensile specimens (25.4 mm long, 0.76 x 5 mm gauge) were prepared with a similar finish. Specimens were ultrasonically cleaned in acetone and methanol prior to exposure. The 500-h exposures at 300 bar were conducted using research grade (RG) CO_2 in a vertically-oriented autoclave (~266 mm x 83 mm inner diameter) fabricated from N07208. Specimens were held in an N07208 sample rack and the fluid flow rate was ~2 ml/min with additional details provided elsewhere[17,20,21]. The specimens were slowly heated to temperature in sCO_2 over several hours (~2°C/min) using a three-zone furnace. After holding at temperature ±1°C for 500 h, the autoclave was then cooled to room temperature. The controlled impurity experiments used two pumps for sCO_2 and H_2O, and O_2 was added as a CO_2–O_2 gaseous mixture from a high pressure cylinder. Based on gas flow rates, the O_2 was calculated as 1.0 ± 0.2% and the H_2O content as 0.1 ± 0.05% with the largest variations associated with issues with filters, valves and changing sCO_2 cylinders (usually twice per 500-h cycle).

The specimens were weighed before and after exposure using a Mettler Toledo model XP205 balance with an accuracy of ±0.04 mg or ~0.01 mg/cm^2. Room temperature tensile tests used a strain rate of 0.015/min per ASTM E8-13. Bulk C was measured using combustion analysis and C profiles were

Table 1
Alloy chemical compositions (weight %)(1)

Alloy	UNS#	Fe	Cr	Ni	Mo	Mn	Si	C	S(ppm)	Other
Gr.91	K91560	88.8	8.6	0.3	0.9	0.46	0.35	0.10	6	0.2V,0.06Nb,0.045N
12CrCoW		83.3	11.5	0.4	0.4	0.38	0.42	0.12	3	1.6W,1.5Co,0.2V,0.04N
316H	S31609	69.5	16.3	10.0	2.0	0.84	0.46	0.041	6	0.3Cu,0.3Co,0.04N
709	S31025	51.3	20.1	25.2	1.5	0.89	0.41	0.064	3	0.2Nb,0.06Cu,0.15N

(1) measured by inductively coupled plasma analysis and combustion analysis
< indicates below the detectability limit of <0.01%

acquired via electron microprobe analysis (EPMA) using a JEOL model 8200 equipped with 5 tunable wavelength dispersive spectrometers. EDS spectra were acquired and processed using a Thermo Scientific Pathfinder EDS system. The accelerating voltage was set to 20 kV and the beam current was 50 nA. Pure standards were used to calibrate all elements. Unknown and standard intensities were corrected for deadtime. Standard intensities were corrected for standard drift measured between the beginning and end of the run. Interference corrections were applied to Mn K_α for interference by Cr K_β and a ZAF algorithm was used[25]. For thin reaction products, Cu plating was used before sectioning for metallography. Reaction product thickness was measured using image analysis software with ~30 measurements per specimen.

RESULTS

Examples of the mass change data in 300 bar RG sCO_2 are shown in Figure 1. The 550°C data were previously presented[26]. The results from 5-6 specimens of each alloy at each condition are presented using box and whisker plots with the median values shown. One specimen of each alloy was removed after 500 h for characterization. The 9-12%Cr steel specimens showed the highest mass gains at each temperature. The addition of impurities (shaded boxes) resulted in an initial mass increase at 450°C compared to the mass change without impurities for all of the alloys. At 650°C, scale spallation was evident for these specimens which affected the values and distribution, Figure 1b. For the S31609 specimens, a uniform mass loss was observed with the addition of impurities. Even for the S31025 specimens, increases were observed at both temperatures with the addition of impurities.

Parabolic rate constants were calculated by plotting the median data points vs. the square root of time[27]. Figure 2 is an Arrhenius plot with the measured RG sCO_2 rates in this study (large open symbols) compared to previous values (small open symbols)[11,21]. The change from 8.6% to 11.5% Cr in the FM steels had little effect on the measured rates, presumably because the Cr mobility is slow in this temperature range[28]. Without impurities, the rates were very low for both austenitic steels at 450° and 550°C and consistent with values measured for Ni-based alloys[21,29]. As noted previously[26], accelerated oxidation of S31609 specimens was observed at 650°C in RG sCO_2 but not for the S31025

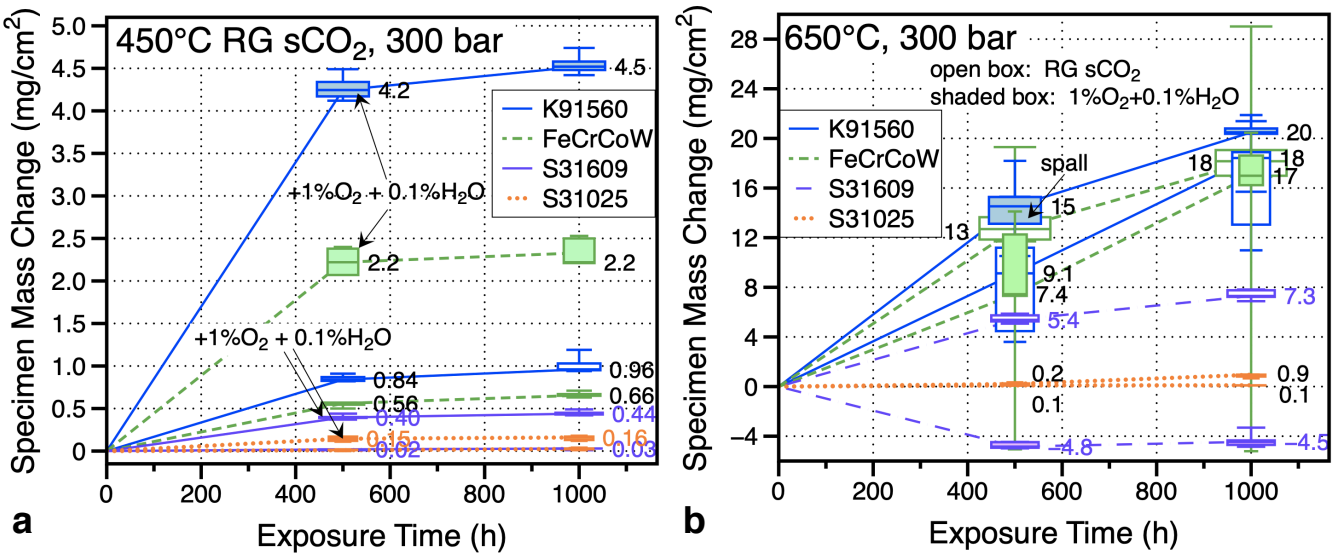

Figure 1. Specimen mass gain during 500-h cycles in 300 bar RG sCO_2 (a) 450° and (b) 650°C. Box and whisker plots show data for 5-6 specimens exposed and the median values are shown.

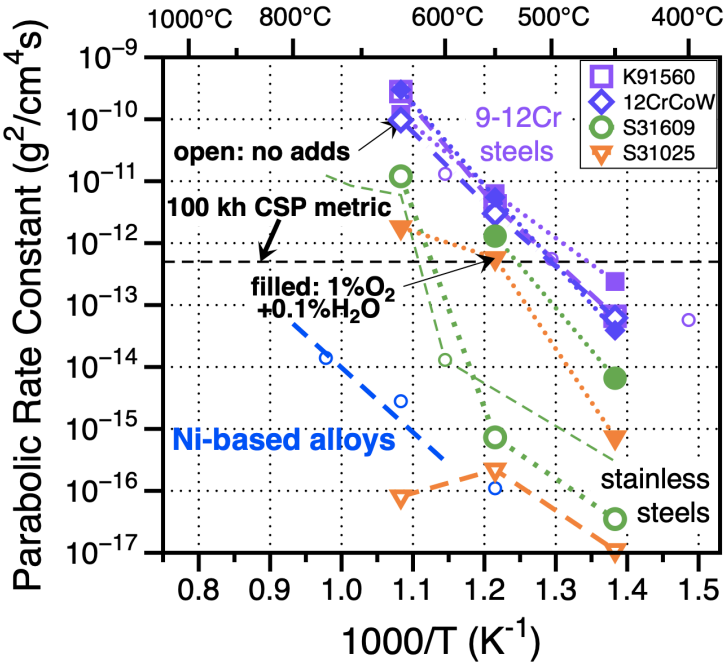

Figure 2: Arrhenius plot of literature values and rate constants from this study in 300 bar RG CO_2 (open symbols) and RG sCO_2 with 1%O_2 + 0.1%H_2O (solid symbols).

specimens. This acceleration in rate has been observed in previous sCO_2 studies[11,30]. With the addition of impurities, very little change in the rates was observed for the FM steels, Figure 2. However, for the austenitic steels, substantial increases were observed, although no rate was calculated for S31609 at 650°C because of the mass losses measured.

Scale cross-sections for the 1000 h exposures in RG sCO_2 were presented previously[31]. Figure 3 shows cross-sections after 1000 h exposures in sCO_2 with impurities at each temperature and then compares the 650°C results to those in RG sCO_2. The oxide thicknesses are generally consistent with the mass change data. At 450°C, a thicker scale was formed on the K91560 specimen compared to the FeCrCoW specimen and these were both much thicker than the scales formed on the austenitic steels. Figure 4 shows oxide scale thickness measurements after 1000 h at each condition. For the FM steels exposed at 550°C, the scales were similar in thickness to those formed at 450°C, Figure 4b. However, the oxides formed at 550°C appeared denser. For the very thick oxides formed at 650°C, it is easier at this magnification to see the duplex Fe-rich oxide microstructure formed on the FM steels as well as an internal oxidation layer at the metal-oxide interface. The light microscopy images show a contrast between the outermost hematite layer, an underlying magnetite layer and the inner $(Fe,Cr)_3O_4$ layer that has been previously identified[12,23,32]. Compared to the oxide formed in RG sCO_2 without impurities, the hematite layer is not present when the impurities are not present.

For the austenitic steels, higher magnification was used in most cases for the thinner reaction products. Oxide layers were not distinct at 450°C, but a thin Cr-rich oxide formed on the S31025 specimen, consistent with the small mass gain. After exposure at 550°C, both the S31609 and S31025 specimens appeared to form a duplex scale, perhaps with a hematite outer layer on the S31609 specimen. After exposure at 650°C, there was a clear difference between the thin Cr-rich oxide scale formed without impurities and the duplex scale formed when impurities were added. For the S31609 specimens exposed at 650°C, a thick Fe-rich duplex scale was formed with and without impurities. In both cases, the outer layer appears to have spalled. In general, scale spallation after exposures at 650°C makes

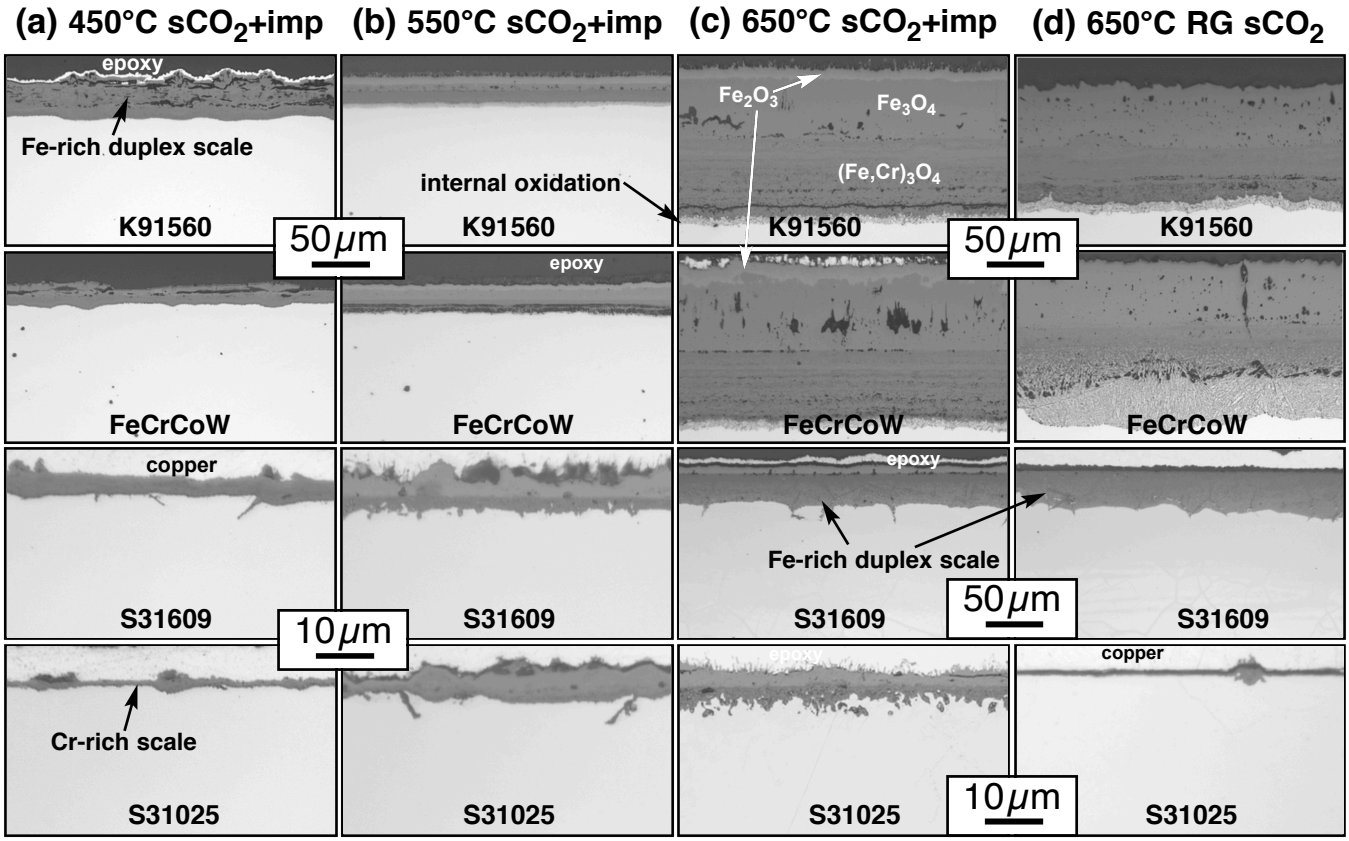

Figure 3: Light microscopy of polished cross-sections of specimens of four steels after 500 h exposures in 300 bar RG sCO_2 (a) 450°C with 1%O_2+0.1%H_2O, (b) 550°C with 1%O_2+0.1%H_2O, (c) 650°C with 1%O_2+0.1%H_2O and (d) 650°C (no impurities).

the scale thickness measurements difficult and not easily comparable to the other alloys.

Figure 5a compares the room temperature tensile properties of the four alloys after 1000 h exposures at each temperature with the as-received properties and the properties after a 1000 h anneal in an argon-filled quartz ampoule at 650°C. At 450°C, the results were similar before and after exposure except for a drop in 0.2% yield strength for the K91560 specimen. After exposure at 550°C, there

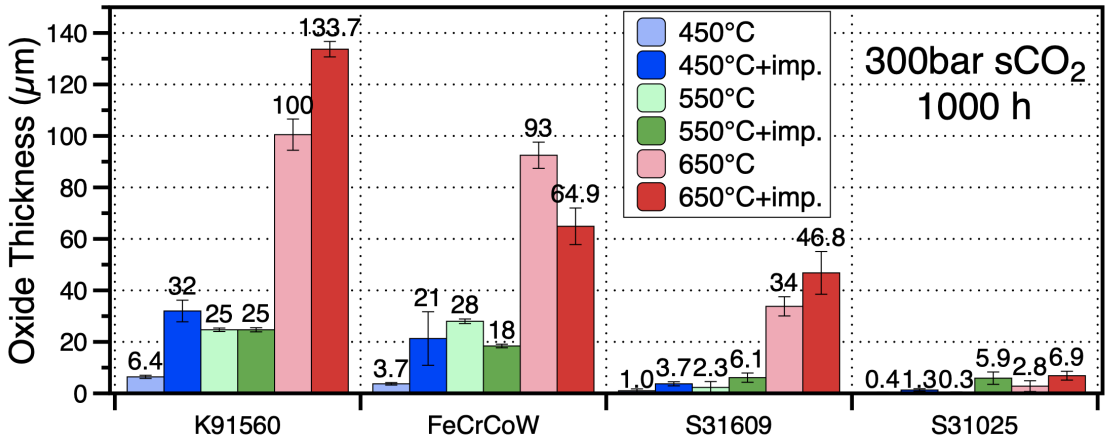

Figure 4: Average oxide thickness after 500 h exposure in 300 bar RG CO_2 at each condition. The whiskers show one standard deviation.

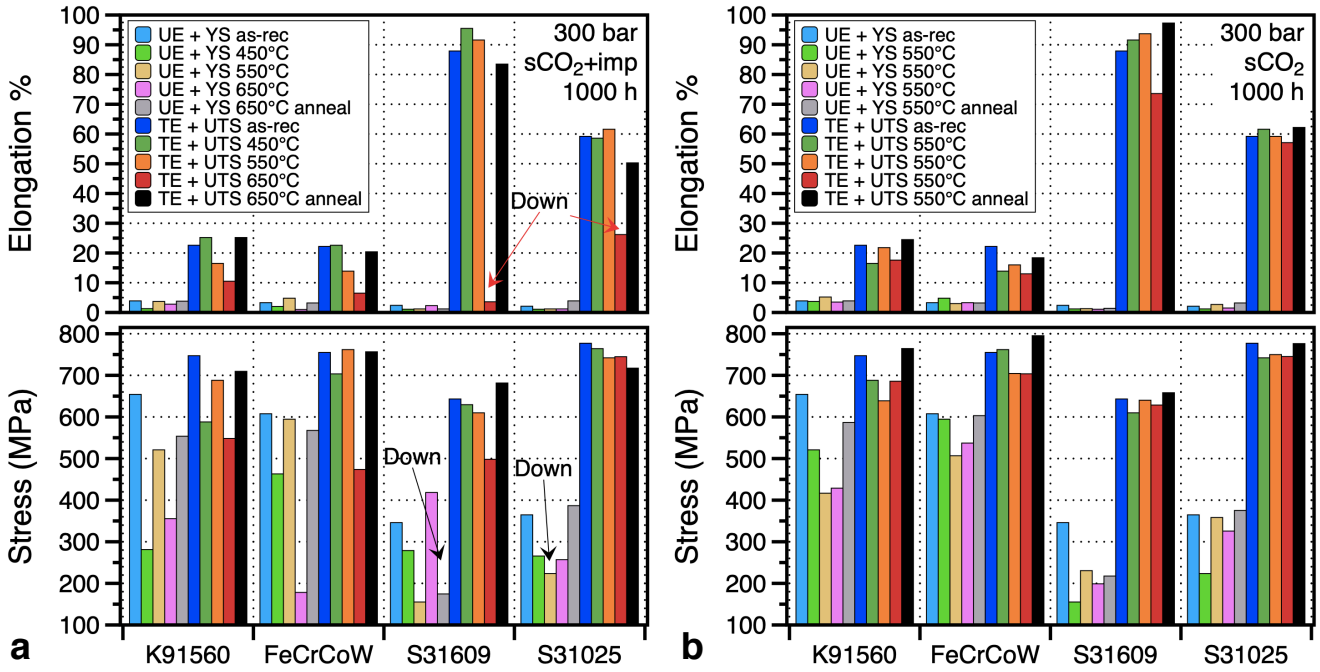

Figure 5: Room temperature tensile properties of steels including uniform (UE) and total elongation (TE), 0.2% yield stress (YS) and ultimate tensile stress (UTS) (a) before and after 1000 h exposures in RG sCO_2 with impurities and (b) triplicate specimens after 1000 h exposures at 550°C in RG sCO_2 with impurities. Comparisons are shown for 1000 h thermal anneals at 550° and 650°C.

appeared to be a decrease in ductility for both FM steels. Because these are only single specimens, changes are difficult to assess. In Figure 5b, three specimens of each alloy exposed for 1000 h at 550°C were tested and compared to results from a 1000 h anneal at 550°C. Based on the three experiments, there does appear to be some degradation in properties for the FM steels after only 1000 h at 550°C. After exposures at 650°C, a drop in ductility was observed for all four alloys with the largest drop for the S31609 specimen, Figure 5a. A similar drop in total elongation was observed for S31609 after exposure in RG sCO_2 without impurities[26,31]. The drop in ductility coupled with an increase in yield strength (only observed for S31609) suggests internal carburization[8]. The bulk C content measurements shown in Figure 6 confirm that C ingress occurred for all four alloys in the impure environment at 650°C. As noted previously[26,31], only the thin, Cr-rich scale shown in Figure 3d appeared to prevent C ingress without impurities at 650°C.

Bulk C measurements at lower temperatures did not show any significant increases. Therefore, EPMA was used to measure C profiles. Figure 7a shows the profiles into the alloy for selected K91560 specimens exposed for 1000 h. The large and variable values after exposure at 650°C are consistent with the high C levels reported in Figure 6. After the 450°C exposure, the profile was flat suggesting no C ingress. However, after both 550°C exposures, the elevated C content near the surface suggests C ingress occurred, perhaps at a slightly higher level with impurities present. For the S31609 specimens shown in Figure 7b, no C enrichment was observed for the 450° and 550°C exposures in RG sCO_2. However, there does appear to be a C peak for the 550°C exposure with impurities perhaps suggesting enhanced C uptake with the addition of impurities. In both cases, the measured C values appear much higher than the 0.1% (T91) and 0.04% (316H) bulk C measurement (Table 1 and Figure 6).

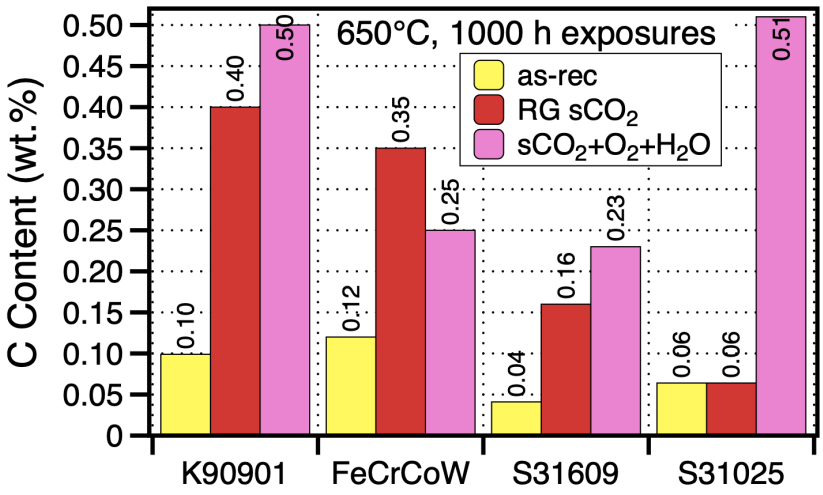

Figure 6: Alloy C content measured after 1000 h exposures in each environment at 650°C using combustion analysis.

DISCUSSION

A combination of reaction rate measurements, room temperature tensile properties and C measurements were used to assess the compatibility of steels in sCO_2 with and without impurities. In general, all of the steels appeared to be degraded at 650°C when impurities were present and none were able to form a Cr-rich oxide scale. Higher Cr content in the FM steel and higher Cr and Ni contents in S31025 did not appear to be effective at 650°C.

Below 650°C, longer exposures may be warranted to assess the sCO_2 effects on mechanical properties and C ingress where small changes were observed after 1000 h. With only two data points, the calculated rates may overestimate the attack. In Figure 1b, the change in median values for S31025 with the addition of impurities was small (2X) after 500 h but 9X after 1000 h. Thus, the steady-state rate may not be reached after only 1000 h for this material. Previously when parabolic behavior was

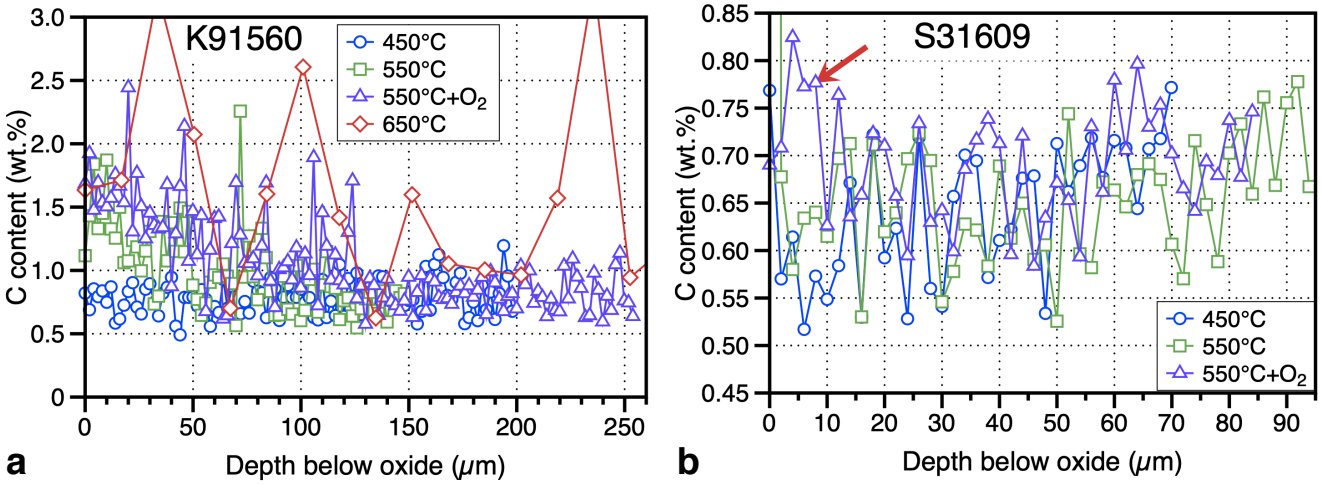

Figure 7. EPMA line profiles after 1000 h exposures in several environments (a) K91560 and (b) S31609. The arrow in (b) notes a peak in C content with sCO_2 impurities at 550°C.

observed in sCO_2, the rates calculated with 2 data points after 1000 h were only marginally different than those calculated after 10,000 h[21]. However, the addition of impurities may result in a longer transient period including the period where the breakdown of the Cr-rich oxide scale occurs. As noted previously at 550°C[26], the S31025 specimens had median values of 0.02 mg/cm^2 in both conditions with larger differences noted after 1000 h with the addition of impurities.

The duplex Fe-rich oxide scales observed here are common to many different environments containing CO_2 and H_2O[10-16,20-23,30-33]. The outer layer remained magnetite in RG sCO_2 which is consistent with the low pO_2 in the sCO_2 environment[34]. With the addition of 1%O_2, the pO_2 increased to 0.01 and hematite was able to form, Figure 3.

The rate constant metric shown in Figure 2 was used to estimate when scale spallation might be significant for a 100,000 h CSP application[21]. The metric was developed for Ni-based alloys but may be relevant for these alloys. The low rates measured for S31025 in RG sCO_2 are unlikely to lead to scale spallation even at long exposure times. However, the thick Fe-rich scales formed on the FM steels may eventually spall, even at 450°C. What the metric does not address is the possible degradation due to C ingress. Thus, the data being collected will be used with the model already developed to better assess long-term behavior at <650°C.

SUMMARY

The sCO_2 compatibility of four steels was investigated in RG sCO_2 and RG sCO_2 with 1%O_2 and 0.1%H_2O additions at 300 bar for 1000 h at 450°-650°C. Mass change was used to calculate parabolic rate constants and post exposure room temperature tensile properties and C contents were measured. After these 1000 h exposures, none of these steels appears to be compatible with impure sCO_2 at 650°C. Some indications of degradation were apparent at 550°C with impurities but a combination of longer exposures and modeling are needed to better assess the long-term performance of these materials and define maximum operating temperatures with and without impurities.

ACKNOWLEDGMENTS

The authors would like to thank B. Johnston, T. M. Lowe and V. Cox for assistance with the experimental work at ORNL. K. A. Kane and E. Lara-Curzio at ORNL provided helpful comments on the manuscript. This research was sponsored by the U.S. Department of Energy, Office of Fossil Energy, Crosscutting Technology Program. This manuscript has been authored by UT-Battelle, LLC under Contract No. DE-AC05-00OR22725 with the U.S. Department of Energy. The United States Government retains and the publisher, by accepting the article for publication, acknowledges that the United States Government retains a non-exclusive, paid-up, irrevocable, world-wide license to publish or reproduce the published form of this manuscript, or allow others to do so, for United States Government purposes. The Department of Energy will provide public access to these results of federally sponsored research in accordance with the DOE Public Access Plan (http://energy.gov/downloads/doe-public-access-plan).

REFERENCES

1. V. Dostal, P. Hejzlar and M. J. Driscoll, “The supercritical carbon dioxide power cycle: Comparison to other advanced power cycles,” Nucl. Technol. 154, 3 (2006): pp.283-301.

2. H. Chen, D. Y. Goswami and E. K. Stefanakos, “A review of thermodynamic cycles and working fluids for the conversion of low-grade heat,” Renewable & Sustainable Energy Reviews 14 (2010): pp.3059-3067.
3. R. J. Allam, M. R. Palmer, G. W. Brown Jr., J. Fetvedt, D. Freed, H. Nomoto, M. Itoh, N. Okita, C. Jones Jr., “High efficiency and low cost of electricity generation from fossil fuels while eliminating atmospheric emissions, including carbon dioxide,” Energy Procedia 37 (2013): pp.1135–1149.
4. B. D. Iverson, T. M. Conboy, J. J. Pasch and A. M. Kruizenga, “Supercritical CO_2 Brayton cycles for solar-thermal energy,” Applied Energy 111, (2013): pp.957-970.
5. I. G. Wright, B. A. Pint, J. P. Shingledecker and D. Thimsen, (2013) “Materials Considerations for Supercritical CO_2 Turbine Cycles,” ASME Paper #GT2013-94941, presented at the International Gas Turbine & Aeroengine Congress & Exhibition, San Antonio, TX, June 3-7, 2013.
6. V. T. Cheang, R. A. Hedderwick, C. McGregor, “Benchmarking supercritical CO_2 cycles against steam Rankine cycles for Concentrated Solar Power,” Solar Energy 113 (2015): pp.199-211.
7. R. Allam, S. Martin, B. Forrest, J. Fetvedt, X. Lu, D. Freed, G. W. Brown, Jr., T. Sasaki, M. Itoh, J. Manning, “Demonstration of the Allam Cycle: An Update on the Development Status of a High Efficiency Supercritical Carbon Dioxide Power Process Employing Full Carbon Capture,” Energy Procedia 114 (2017): pp.5948-5966.
8. H. E. McCoy, “Type 304 Stainless Steel vs Flowing CO_2 at Atmospheric Pressure and 1100-1800°F,” Corrosion 21 (1965): pp.84-94.
9. W. R. Martin and J. R. Weir, “Influence of Chromium Content on Carburization of Chromium-Nickel-Iron Alloys in Carbon Dioxide,” J. Nucl. Mater. 16 (1965): pp.19-24.
10. C. T. Fujii and R. A. Meussner, “Carburization of Fe-Cr Alloys During Oxidation in Dry Carbon Dioxide,” J. Electrochem. Soc. 114 (1967): pp.435-442.
11. T. Furukawa, Y. Inagaki, M. Aritomi, “Compatibility of FBR structural materials with supercritical carbon dioxide,” Progress in Nuclear Energy 53, (2011): pp.1050–1055.
12. F. Rouillard, F. Charton and G. Moine, “Corrosion Behavior of Different Metallic Materials in Supercritical Carbon Dioxide at 550°C and 250 bars,” Corrosion 67, 9 (2011): p.095001.
13. T. Gheno, D. Monceau and D. J. Young, “Kinetics of breakaway oxidation of Fe-Cr and Fe-Cr-Ni alloys in dry and wet carbon dioxide,” Corrosion Science 77 (2013): pp.246-256.
14. R. I. Olivares, D. J. Young, P. Marvig and W. Stein, “Alloys SS316 and Hastelloy-C276 in Supercritical CO_2 at High Temperature,” Oxid. Met. 84 (2015): pp.585–606.
15. Y. Gong, D. J. Young, P. Kontis, Y. L. Chiu, H. Larsson, A. Shin, J. M. Pearson, M. P. Moody and R. C. Reed, “On the breakaway oxidation of Fe9Cr1Mo steel in high pressure CO_2,” Acta Materialia, 130 (2017): pp.361-374.
16. S. Sarrade, D Férona, F. Rouillard, S. Perrin, R. Robin, J.-C. Ruiz, H.-A. Turc, “Overview on corrosion in supercritical fluids,” Journal of Supercritical Fluids, 120 (2017): pp.335–344.
17. B. A. Pint and J. R. Keiser, “Initial Assessment of Ni-Base Alloy Performance in 0.1 MPa and Supercritical CO_2,” JOM 67, 11 (2015): pp.2615-2620.
18. J. Mahaffey, D. Adam, A. Brittan, M. Anderson and K. Sridharan, “Corrosion of Alloy Haynes 230 in High Temperature Supercritical Carbon Dioxide with Oxygen Impurity Additions,” Oxidation of Metals 86 (2016): pp.567-580.
19. R. P. Oleksak, J. H. Tylczak, C. S. Carney, G. R. Holcomb and O. N. Dogan, “High-Temperature Oxidation of Commercial Alloys in Supercritical CO_2 and Related Power Cycle Environments,” JOM 70 (2018): pp.1527-1534.
20. B. A. Pint, J. Lehmusto, M. J. Lance and J. R. Keiser, “The Effect of Pressure and Impurities on Oxidation in Supercritical CO_2,” Mater. Corros. 70 (2019): pp.1400-1409.
21. B. A. Pint, R. Pillai, M. J. Lance and J. R. Keiser “Effect of Pressure and Thermal Cycling on Long-Term Oxidation in CO_2 and Supercritical CO_2” Oxidation of Metals 94 (2020): pp.505–526.

22. A. M. Pritchard, J. E. Antill, K. R. J. Cottell, K. A. Peakall and A. E. Truswell, “The Mechanisms of Breakaway Oxidation of Three Mild Steels in High-Pressure CO2 at 500°C,” Oxidation of Metals 9 (1975): pp.181-214.
23. J. P. Shingledecker, B.A. Pint, A.S. Sabau, A.T. Fry and I.G. Wright, “Managing Steam-Side Oxidation and Exfoliation in USC Boiler Tubes,” Advanced Materials and Processing, 171(1) (2013): pp.23-25.
24. M. N. Gussev, J. T. Busby, K. G. Field, M. A. Sokolov and S. E. Gray, “Role of Scale Factor During Tensile Testing of Small Specimens,” in Small Specimen Test Techniques: 6th Volume, STP 1576, M. A. Sokolov and E. Lucon, Eds., pp. 31–49, ASTM International, West Conshohocken, PA 2014.
25. J. T. Anderson, “Quantitative analysis of silicates and oxide minerals: Comparison of Monte-Carlo, ZAF and Phi-Rho-Z procedures,” in Microbeam Analysis–1988, D. E. Newbury, ed., San Francisco Press, San Francisco, CA, 1988, pp.239-246.
26. B. A. Pint, R. Pillai and J. R. Keiser, “Compatibility of Steels in Supercritical CO_2 at 450°-650°C,” Paper C2021-16724, Houston, TX, presented virtually at Corrosion 2021, April 2021.
27. B. Pieraggi, "Calculations of Parabolic Reaction Rate Constants," Oxid. Met., 27 (1987): p.177.
28. Zs. Tökei, K. Hennesen, H. Viefhaus, H. J. Grabke, "Diffusion of Chromium in Ferritic and Austenitic 9-20 Wt.% Cr Steels," Materials Science Technology 16, (2000): pp.1129-1138.
29. V. Dheeradhada, A. Thatte, M. Karadge and M Drobnjak, “Corrosion of Supercritical CO_2 Turbomachinery Components,” in Proceedings of the EPRI International Conference on Corrosion in Power Plants, Oct. 2016, San Diego, CA.
30. G. Cao, V. Firouzdor, K. Sridharan, M. Anderson and T. R. Allen, “Corrosion of austenitic alloys in high temperature supercritical carbon dioxide,” Corrosion Science 60 (2012): pp.246-255.
31. B. A. Pint, R. Pillai and J. R. Keiser, “Effect of Supercritical CO_2 on Steel Ductility at 450°-650°C” ASME Paper #GT2021-59383, for Turbo Expo 2021 Virtual Conference and Exhibition, June 11-15, 2021.
32. L. Tan, M. Anderson, D. Taylor, T. R. Allen, “Corrosion of austenitic and ferritic-martensitic steels exposed to supercritical carbon dioxide,” Corrosion Science 53 (2011): pp.3273-3280.
33. S. R. J. Saunders, M. Monteiro and F. Rizzo, “The oxidation behaviour of metals and alloys at high temperatures in atmospheres containing water vapour: A review,” Progress in Materials Science 53 (2008): pp.775-837.
34. B. A. Pint, R. G. Brese and J. R. Keiser, “Effect of Pressure on Supercritical CO_2 Compatibility of Structural Alloys at 750°C,” Materials and Corrosion 68 (2017): pp.151-158.